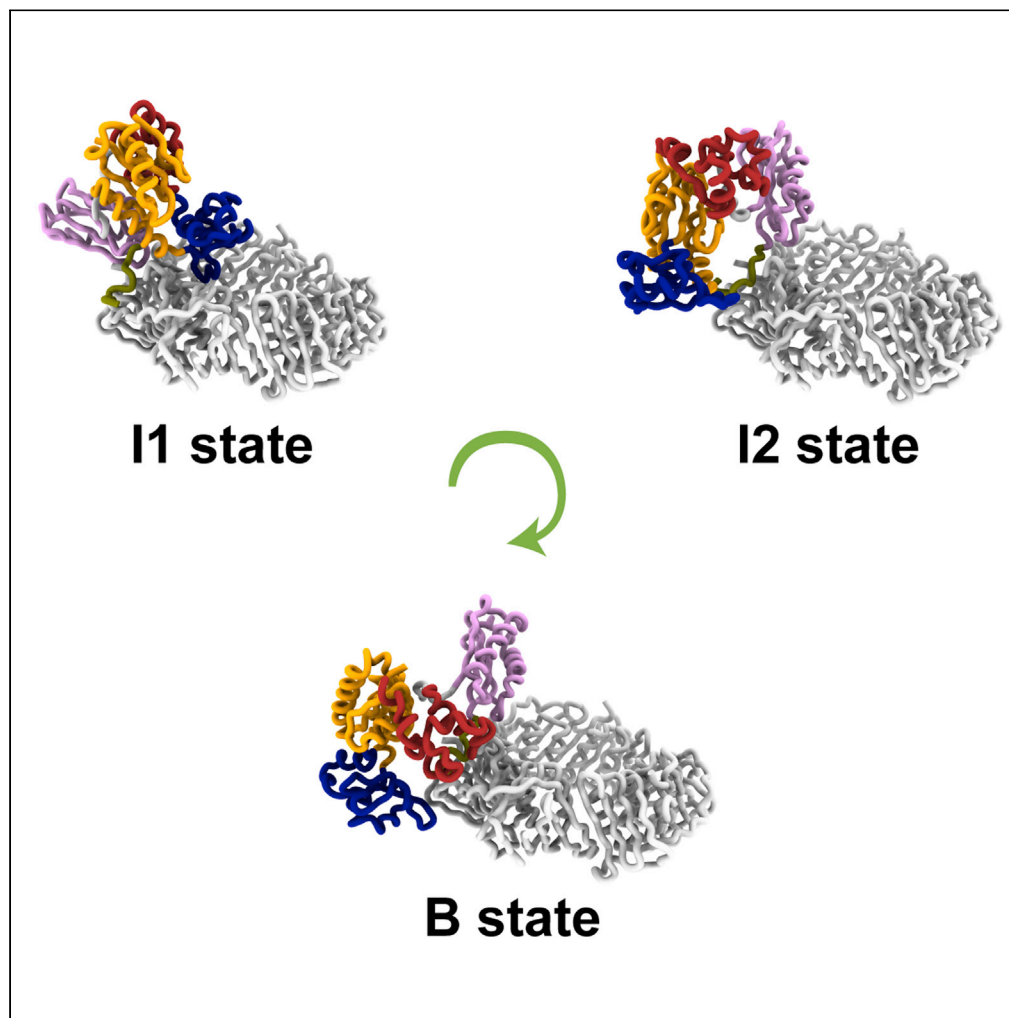


Article

Binding-Induced Conformational Changes
Involved in Sliding Clamp PCNA and DNA
Polymerase DPO4

Wen-Ting Chu,
Zucai Suo, Jin
Wang

jin.wang.1@stonybrook.edu

HIGHLIGHTS

The mechanism of DPO4
binding to PCNA ring and
PCNA dimer is
investigated

Two important
intermediate states are
found before reaching the
final bound state

Both PCNA3 and DPO4
can influence the PCNA12
planar conformation

Chu et al., iScience 23, 101117
May 22, 2020 © 2020 The
Author(s).
[https://doi.org/10.1016/
j.isci.2020.101117](https://doi.org/10.1016/j.isci.2020.101117)

Article

Binding-Induced Conformational Changes Involved in Sliding Clamp PCNA and DNA Polymerase DPO4

Wen-Ting Chu,¹ Zucai Suo,² and Jin Wang^{3,4,*}

SUMMARY

Cooperation between DNA polymerases and DNA sliding clamp proteins is essential for DNA replication and repair. However, it is still challenging to clarify the binding mechanism and the movements of Y-family DNA polymerase IV (DPO4) on the proliferating cell nuclear antigen (PCNA) ring. Here we develop the simulation models of DPO4–PCNA123 and DPO4–PCNA12 complexes and uncover the underlying dynamics of DPO4 during binding and the binding order of the DPO4 domains. Two important intermediate states are found on the free energy surface before reaching the final bound state. Our results suggest that both PCNA3 and DPO4 can influence the PCNA12 planar conformation, whereas the impact of PCNA3 on PCNA12 is more significant than DPO4. These findings provide the crucial information of the conformational dynamics of DPO4 and PCNA, as well as the clue of the underlying mechanism of the cooperation between DPO4 and PCNA during DNA replication.

INTRODUCTION

DNA polymerases, which catalyze synthesis of poly-deoxyribonucleotides from mono-deoxyribonucleoside triphosphates (dNTPs), are crucial for DNA replication, repair, and, in some cases, cell differentiation (Steitz, 1999). In living cells, specialized DNA polymerases including mainly Y-family DNA polymerases can bypass various DNA lesions, although they can replicate undamaged DNA with low-fidelity and poor processivity (Ohmori et al., 2001; Friedberg et al., 2002). The Y-family DNA polymerases share little sequence identity with high-fidelity replicative DNA polymerases in the A- and B-families. However, the Y-family DNA polymerases have a conserved right-handed polymerase core of palm, thumb, and finger domains (Ling et al., 2001; Zhou and Elledge, 2000; Silvian et al., 2001; Trincao et al., 2001). There is an additional little finger (LF) domain located at the C terminus of the Y-family DNA polymerases, which has been shown to increase their overall binding affinity to DNA by contacting the DNA major groove (Ling et al., 2001; Silvian et al., 2001; Boudsocq et al., 2004).

Sulfolobus solfataricus DNA polymerase IV (DPO4) is a representative member of the Y-family DNA polymerases, and both its structure and functions have been investigated in great depth (Wong et al., 2008; Ling et al., 2001; Xing et al., 2009; Wang et al., 2012; Chu et al., 2014; Chu and Wang, 2018, 2020). In crystal structures, DPO4 exhibits large conformational changes upon binding to DNA (from apo state to DNA-bound state), in which the LF domain moves from close to the thumb domain (apo state) to close to the finger domain (DNA-bound state), suggesting the binding-induced “open to closed” mechanism. Similar conformational changes have also been inferred from the crystal structures of Y-family DNA polymerases in other species (Trincao et al., 2001; Uljon et al., 2004). Previous studies have shown that DPO4 is under a conformational equilibrium between multiple states during the DNA-binding process and the distributions of the conformations vary at different binding stages (Wang et al., 2012; Chu et al., 2014). However, a third structural state of DPO4 was reported in 2009, in which the LF domain exhibits a different configuration from that at the apo and DNA-bound states and is located on the surface of the proliferating cell nuclear antigen (PCNA) (Xing et al., 2009).

PCNA is a six-domain ring that clamps DNA and provides a platform for DNA-processing enzymes, such as DNA polymerases, DNA ligase I, and Flap endonuclease 1 (Fen1) in almost every DNA metabolic process, including replication, repair, recombination, modification, and cell cycle regulation (Kelman, 1997;

¹State Key Laboratory of Electroanalytical Chemistry, Changchun Institute of Applied Chemistry, Chinese Academy of Sciences, Changchun, Jilin 130022, China

²Department of Biomedical Sciences, College of Medicine, Florida State University, Tallahassee, FL 32306-4300, USA

³Department of Chemistry & Physics, State University of New York at Stony Brook, Stony Brook, NY 11794-3400, USA

⁴Lead Contact

*Correspondence: jin.wang.1@stonybrook.edu
<https://doi.org/10.1016/j.isci.2020.101117>



Tsurimoto, 1999; Dieckman et al., 2012; Georgescu et al., 2008; Matsumiya et al., 2001; Pascal et al., 2006). The PCNA ring surface facing the primer-extension direction forms a platform that tethers DNA-modifying enzymes (PCNA-interacting proteins, PIPs) on the DNA substrate as the clamps move along the DNA (Waga and Stillman, 1998; Warbrick, 2000). The PIPs interact with PCNA via the well-conserved PIP-box motif, Qxx(M/L/I)xxF(Y/W) (Warbrick, 2000; Dalrymple et al., 2001). Previous structural studies have shown that the PIP-box binds to the interdomain connecting loop (IDCL) of the PCNA ring and its proximal hydrophobic cavity (Gulbis et al., 1996). In addition, it has been found that the PCNA heterotrimeric ring (formed by three monomers PCNA1, PCNA2, and PCNA3) from *S. solfataricus* binds and stimulates Fen1, DNA polymerase B1 (Pol B1), DNA ligase 1, as well as DPO4 through their PIP-box regions (Dionne et al., 2003, 2008; Dore et al., 2006; Xing et al., 2009). The crystal structure of the full-length DPO4 (352 a.a.) and *S. solfataricus* PCNA (two monomers, PCNA12) complex (PCNA12–DPO4) was resolved in 2009 (Xing et al., 2009). Both native PAGE and DNA mobility shift assay results indicate that PCNA1 is a minimum and sufficient DPO4-binding partner (Xing et al., 2009). In this structure, the C-terminal PIP-box (residues 342–352) of DPO4 becomes ordered in the complexed structure with PCNA, whereas it is disordered in the *apo* and DNA-bound structures (Demarest et al., 2002). Thus, two intrinsically flexible hinge regions have been found in the DPO4. One is located on the flexible linker between the core and the LF domain, and the other is located at the C-terminal end of the LF domain. However, other DNA-processing enzymes do not have the first hinge region and the major conformational changes found in the Y-family polymerases (Silvian et al., 2001; Uljon et al., 2004; Wong et al., 2008; Ling et al., 2004). Moreover, comparison between the *apo* PCNA12 and the DPO4–PCNA12 complex structures has revealed a slightly off-planar movement of the PCNA1–PCNA2 plane in the DPO4-bound PCNA12 structure (Xing et al., 2009).

Investigation of the underlying mechanisms and details of the binding process between PCNA and DPO4 is still challenging. Although molecular dynamics (MD) simulations provide a good way to study the important interactions of the protein systems and collect atomic structural information, it is rather time consuming for conventional MD simulations to deal with the protein systems with such large-scale conformational changes during binding. In the present study, structure-based models based on the energy landscape theory (Bryngelson and Wolynes, 1987; Shoemaker et al., 2000; Clementi et al., 2000; Turjanski et al., 2008; Ganguly et al., 2013; Lu and Wang, 2008) as well as the two-basin (and even multi-basin) models (Chu and Voth, 2007; Lu and Wang, 2008; Whitford et al., 2007; Okazaki et al., 2006; Chu et al., 2017; Chu and Wang, 2018; Liu et al., 2017) are developed for effectively sampling the PCNA–DPO4 binding process associated with the large conformational changes on DPO4. We develop a variety of different binding systems of DPO4 complexed with either PCNA12 or PCNA123, respectively. By performing the thermodynamic and kinetic binding MD simulations, we show the dynamic distributions of both DPO4 and PCNA conformations and identify the critical interactions and residues during binding. Our results uncover the underlying mechanisms and the details of different conformational changes during the DPO4 and PCNA binding process, thus making a significant contribution to the research of DNA replication.

RESULTS AND DISCUSSION

Finger Domain Moves from Center to Side of PCNA

DPO4 is a Y-family polymerase that has a polymerase core consisting of palm, finger, and thumb domains in addition to a fourth domain known as the little finger (LF) domain. In the structure of PCNA12–DPO4 (PDB: 3FDS), all the native contacts exist between three domains (finger, thumb, LF) as well as PIP-box of DPO4 and PCNA1 monomer (see Figure 1). Considering the native structure of PCNA12–DPO4, the PCNA1 monomer is crucial for the binding of DPO4. The different forms of DPO4 and its domain information are illustrated in Figure 1. DPO4 undergoes large-scale conformational changes upon DNA binding, with the movement of LF domain connected by the flexible linker loop (colored gray in Figures 1C–1E). In the DNA-bound state (Figure 1D, PDB: 2RDJ), the LF domain moves toward and interacts with the finger domain, binding with the DNA ligand strongly (“closed” form), whereas in the *apo* form (Figure 1E, PDB: 2RDI), the LF domain changes to have strong interactions with the thumb domain (“open” form). When DPO4 binds with PCNA (Figure 1C, PDB: 3FDS), the LF domain moves away from the other domains to get interactions with PCNA. In addition, the PIP-box of DPO4 is important for DPO4 binding to PCNA12. More than half (60.8%) of the native contacts between DPO4 and PCNA12 are located on this PIP-box region (Figure 1F). If we superimpose these different forms of DPO4 together, we can see that the rotating angle of LF domain continues to change throughout them, whereas the other domains (palm, finger, and thumb) almost remain unchanged.

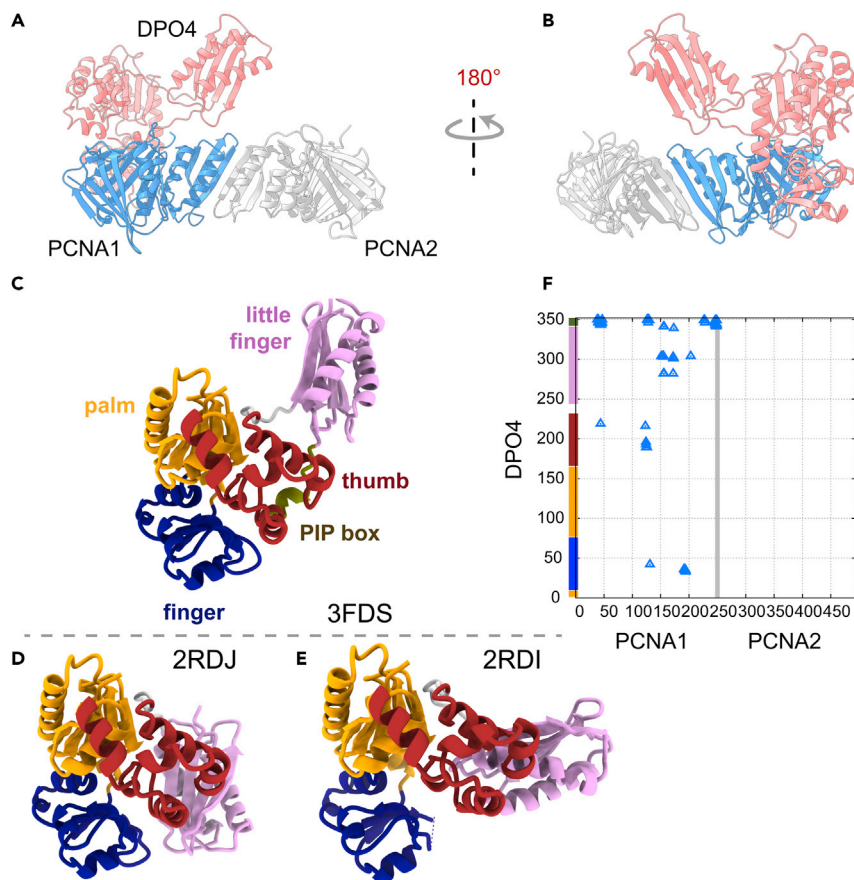


Figure 1. Different Forms of DPO4

The PCNA12–DPO4 structure (PDB: 3FDS, A and B), the important DPO4 forms and domains (C–E), and the native contact map of the interactions between DPO4 and PCNA12 in PDB: 3FDS (F). Here, DPO4 has three main forms in crystal structures: the *apo* form (PDB: 2RDI), the DNA-bound form (PDB: 2RDJ), and the PCNA12-bound form (PDB: 3FDS). DPO4 contains palm (1–9, 77–165), finger (10–76), thumb (166–232), and LF (244–341) domains, as well as a PIP-box (342–352). The binding partners of DPO4 in the crystal structures (DNA or PCNA12) are not shown in (C)–(E). DPO4 sequence (y axis) is colored for different domains in (F), with the same color in (C)–(E). The native contacts are determined with Shadow Algorithm [Noel et al. \(2012, 2010\)](#).

After modeling the system of PCNA123 and DPO4, replica-exchange molecular dynamics (REMD) simulations were performed to obtain the free energy profiles. Room-temperature free energy profiles were extracted and projected onto several reaction coordinates. Here we define Q_{inter} PCNA–DPO4 as the fraction of native contacts between PCNA and DPO4 (obtained from PDB: 3FDS, see [Figure 1F](#)); Q_{speci} DPO4 as the fraction of the native contacts that are specific for DPO4 conformational changes between *apo* DPO4 and PCNA-bound forms (the intra-chain native contacts of DPO4 belong to only one form of DPO4 [*apo* DPO4 or PCNA12-bound DPO4]). As shown in [Figure 2A](#), at room temperature, there is one basin with the lowest free energy (B state) as well as two basins with slightly higher free energy (I1 and I2 states). The B state (0.0 kT) is located at about $Q_{inter} = 0.86$, $Q_{speci} = 0.76$, where DPO4 is considered to fully bind with PCNA123. The other two intermediate states I1 and I2 are located at about $Q_{inter} = 0.62$, $Q_{speci} = 0.82$ and $Q_{inter} = 0.70$, $Q_{speci} = 0.72$, with free energy 0.7 and 0.4 kT higher than that of the B state, respectively. Although these three states have similar heights and locations on the free energy surface, PCNA123-bound DPO4 in these states exhibits different configurations and binding poses (see [Figure 3A](#)). In the B state, the finger, thumb, and LF domains of DPO4 have interactions with PCNA123 ([Figure 3B](#)), consistent with the PDB: 3FDS structure. In the I1 state, the DPO4 rotates on the axis of the PIP-box with the finger domain toward the center of the PCNA ring. The palm, thumb, and LF domains move away from their original binding sites ([Figure 3C](#)). In the I2 state, the finger and LF domains stay at their original binding sites while the thumb domain moves away from the PCNA ring ([Figure 3D](#)).

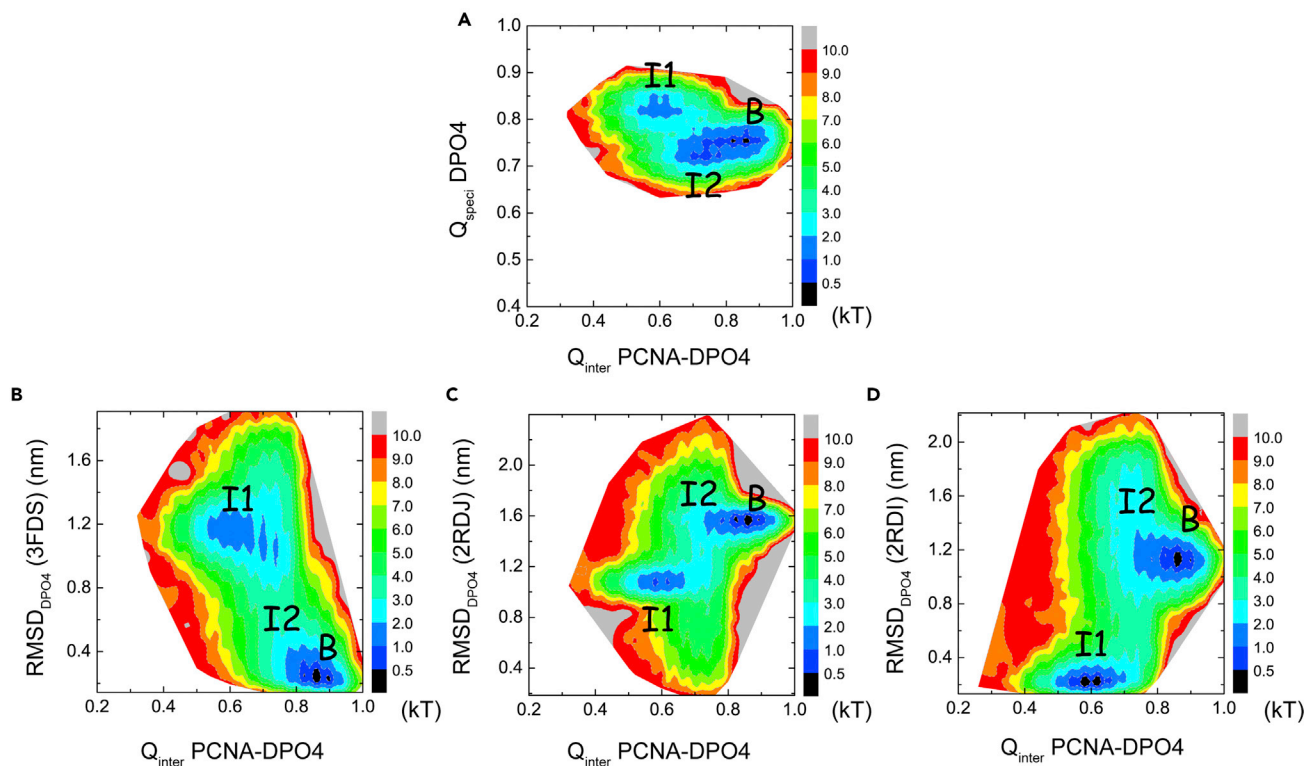


Figure 2. Free Energy Profiles of PCNA123 and DPO4 Complex

Free energy profile as a function of (A) the fraction of native contacts between PCNA and DPO4 (Q_{inter} PCNA–DPO4) and the fraction of specific native contacts of DPO4 (Q_{speci} DPO4), (B) Q_{inter} PCNA–DPO4 and RMSD of DPO4 with respect to the DPO4 in PDB: 3FDS ($RMSD_{DPO4}$ [PDB: 3FDS]), (C) Q_{inter} PCNA–DPO4 and RMSD of DPO4 with respect to the DPO4 in PDB: 2RDJ ($RMSD_{DPO4}$ [PDB: 2RDJ]), (D) Q_{inter} PCNA–DPO4 and RMSD of DPO4 with respect to the DPO4 in PDB: 2RDI ($RMSD_{DPO4}$ [PDB: 2RDI]). These free energy data were extracted at $T = 1.24$ (in reduced unit, mimicking the room temperature) with the weighted histogram analysis method (WHAM) Yeh et al. (2008); Kumar et al. (1992). The free energy is in unit of kT.

In all these three states, the C-terminal PIP-box region of DPO4 strongly and steadily binds to the surface of PCNA1 (see Figure 3A). The PIP-box (342–352, DPO4) is a well-conserved domain in PIPs. It has been observed experimentally that the C-terminal PIP-box of DPO4 is essential and sufficient for PCNA–DPO4 binding (Xing et al., 2009). However, this part is missing in the PDB: 2RDI (apo DPO4) and PDB: 2RDJ (DPO4 with DNA) structures. It suggests that the PIP-box of DPO4 acts as an anchor when DPO4 moves on the surface of PCNA123.

Moreover, we also compare the configuration of DPO4 at these states by projecting the free energy on the reaction coordinates of Q_{inter} PCNA–DPO4 and root-mean-square deviation (RMSD) of DPO4. We calculated the RMSD values of DPO4 with respect to the DPO4 in PDB: 3FDS (Figure 2B), PDB: 2RDJ (Figure 2C), and PDB: 2RDI (Figure 2D), respectively. It should be noted that the DPO4 at B state is close to the configuration of DPO4 in PDB: 3FDS (PCNA12-bound DPO4). The I1 state seems to be similar to the configuration of DPO4 in PDB: 2RDI (apo DPO4). In order to demonstrate the internal conformational changes of DPO4, we superimposed the representative frames of the three main states with the experimental structures of DPO4 (Figure 4A). The large conformational changes within DPO4 occur mainly on the LF domain, which is linked to the core part (palm, finger, and thumb domains) with a flexible loop region (colored gray in Figures 1C–1E). The LF domain of DPO4 in the I1 state is between that of DPO4 in PDB: 3FDS and PDB: 2RDJ and close to the DPO4 in PDB: 2RDI. The I2 state is difficult to be distinguished from the B state on the free energy surface of the Q_{inter} PCNA–DPO4 and RMSD of DPO4. It seems that, in the I2 state, the LF domain is different from that in other configurations of DPO4 but fairly close to the PDB: 3FDS structure (see Figure 4A).

In the previous works of PCNA and DPO4 complex (Xing et al., 2009), the researchers estimated the different conformations of DPO4 bound to PCNA when there is a section of dsDNA occupied in the center of PCNA ring. However, the structure of PCNA–DPO4–dsDNA complex (and that of the PCNA–dsDNA complex) has

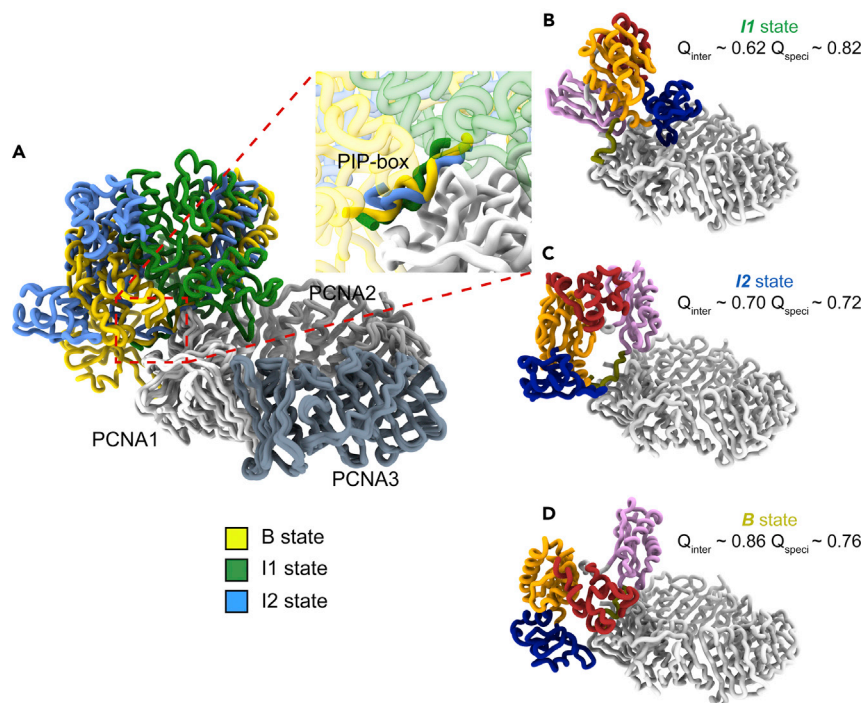


Figure 3. The Representative Configurations of PCNA123–DPO4 Located at the Free Energy Basins (I1, I2, and B States)

For these configurations, the PCNA123 ring is superimposed and drawn with the same color. In (A), DPO4 structures in I1, I2, and B states are colored in green, blue, and yellow, respectively. In addition, the PIP-box region is highlighted in the zoom-in window of (A). In (B)–(D), DPO4 domains are colored the same as in Figure 1.

yet to be resolved. All the structures in this paper were constructed using the published structures PDB: 2NTI/PDB: 2HII (*apo* PCNA123), PDB: 3FDS (DPO4–PCNA12), and PDB: 2RDI (*apo* DPO4). Our simulations here suggest that the I1 state may be an intermediate state between the extended form and the active form of DPO4 mentioned in this paper, close to the configuration of the *apo* form attaching to the PCNA ring, because the DPO4 starts to rotate and the core domain moves to the center hole of the PCNA ring.

DPO4 Binds to PCNA12 through Similar Intermediates

Previous experimental data have shown that PCNA1 and PCNA2 first form a stable heterodimer (PCNA12), which is then capable of recruiting PCNA3 to complete the ring structure (Xing et al., 2009; Vladena et al., 2008). In addition, only PCNA12 and DPO4 complex but no PCNA123 and DPO4 complex has been obtained. Here, in order to explore the function of PCNA3 on the PCNA ring, both PCNA12–DPO4 and PCNA123–DPO4 models were prepared for the REMD simulations. The PCNA12–DPO4 model has the same parameters as the PCNA123–DPO4 model, although the former does not include PCNA3.

After simulations, the free energy at room temperature was extracted and projected on the same reaction coordinates as above. Similar to PCNA123–DPO4, the PCNA12–DPO4 system also exhibits three states, one bound state as well as two intermediate states (B, I1, and I2 states), on the free energy surface of DPO4-binding path. As shown in Figure S2, these three states have the same location as in the PCNA123–DPO4 complex. However, the free energy values of these states are slightly different from before. The free energy of the I1 state (0.4 kT) is closer to that of the B state than to that of the I2 state (0.6 kT). This suggests that the PCNA without PCNA3 favors the movement of the finger domain of DPO4 into the center hole of PCNA.

Furthermore, the B state conformations of both PCNA123–DPO4 and PCNA12–DPO4 are very similar to the conformation in PDB: 3FDS, with RMSD values of about 3.72 and 3.07 Å, respectively (as shown in Figure S3).

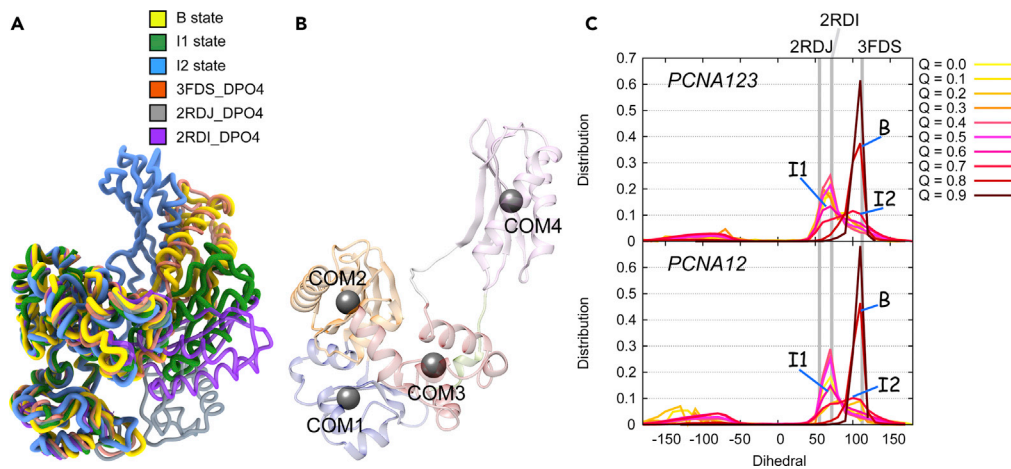


Figure 4. Conformational Changes within DPO4

(A) The superimposed DPO4 structures (DPO4 in B, I1, and I2 states, as well as DPO4 in PDB: 3FDS, PDB: 2RDI, and PDB: 2RDJ PDB structures); (B) some beads indicating the center of mass (COM) positions of finger (COM1), palm (COM2), thumb (COM3), and LF (COM4) on the PCNA12-bound DPO4 structure (PDB: 3FDS); (C) distributions of the dihedral ω of the four domains (finger, palm, thumb, and LF), COM1–COM2–COM3–COM4. The distributions of ω curves in different binding stages are plotted with gradient color (Q and its corresponding color are listed). The curves of I1, I2, and B states are labeled. In addition, the ω values in the apo (PDB: 2RDI), DNA-bound (PDB: 2RDJ), and PCNA-bound (PDB: 3FDS) crystal structures are labeled as gray lines.

In the previous study of the PCNA12–DPO4 structure, the authors identified two intrinsically flexible hinge regions in DPO4 based on the multiple conformations (Ling et al., 2001; Wong et al., 2008; Xing et al., 2009). The main one of these hinges is located on the flexible linker between the core and the LF domain. Consequently, we analyzed the movement of the LF domain with respect to the core part by calculating the dihedral ω of the four domains (finger, palm, thumb, and LF). ω is defined with the center of mass (COM) sites of the finger (COM1), palm (COM2), thumb (COM3), and LF (COM4); see Figure 4B. As shown in Figure 4C, from the beginning of the binding process to the I1 state, the relative positions of the four domains are similar to those in the apo DPO4 structure (PDB: 2RDI); from I1 state to B state, the peak of the ω distribution moves from the position of PDB: 2RDI to PDB: 3FDS; whereas at the bound state, the relative positions of the four domains are close to those in the PCNA12-bound DPO4 structure (PDB: 3FDS). Moreover, with the additional PCNA3, the ω of PCNA123-bound DPO4 has similar changes to that of the PCNA12-bound DPO4. Therefore, when DPO4 binds to PCNA123 or PCNA12, the conformational changes of DPO4 almost keep the same.

Thumb and LF Domains Touch PCNA First

In order to investigate the binding order, we divided the native inter-molecular contacts into several parts (between three domains and PIP-box of DPO4 and PCNA; here the palm domain does not have native inter-molecular contacts with PCNA, see the analysis in the first section of Results and Discussion) and then analyzed their Q values at different stages of the binding path. As shown in Figure 5, here the situations of these native interactions along the binding path of DPO4 to PCNA123 and PCNA12 are similar. At the first stage of binding ($Q_{inter} < 0.1$), the thumb and LF domains of DPO4 touch PCNA123 (or PCNA12) first, whereas the other domains have much lower proportion of interactions with PCNA in this period. At the middle stage of binding ($Q_{inter} \sim 0.1$ – 0.4), PIP-box begins to bind with PCNA, with mean Q increased from about 0.1 to 0.6. The main inter-molecular interactions belong to the LF domain and PIP-box of DPO4. LF domain undergoes two main shifts, one before $Q_{inter} = 0.2$ and the other after $Q_{inter} = 0.2$. After the second shift ($Q_{inter} \sim 0.38$), the mean Q between the LF domain and PCNA decreases to about 0.1. Then the LF domain and PIP-box continue binding to PCNA. At I1 state ($Q_{inter} \sim 0.6$), PIP-box binds almost fully to PCNA, whereas LF binds to PCNA with about half native contacts. The finger and thumb domains have few contacts with PCNA. At I2 state ($Q_{inter} \sim 0.7$), both LF domain and PIP-box bind strongly with PCNA, whereas the finger and thumb domains remain out of the final binding site. After the B state ($Q_{inter} > 0.8$), all the parts of DPO4 find their binding places. These results are consistent with the representative configurations extracted from the trajectory above (Figures 3B–3D).

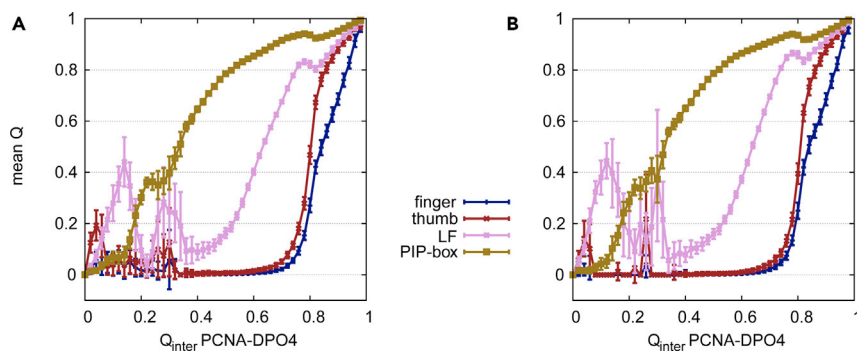


Figure 5. Changes of Native Interactions during Binding

Distribution of native interactions between different domains of DPO4 and PCNA (PCNA123 [A] or PCNA12 [B]) on the binding path. Here, mean fraction of native contacts (Q) of each domain and its standard error are calculated. There are no native contacts between the palm domain and PCNA. As a result, only the Q informations of the other four domains are shown in this figure. Note that all the native contacts between PCNA and DPO4 locate on the PCNA1 monomer (see the first section of [Results and Discussion](#)).

Furthermore, the contact map between PCNA and DPO4 can clearly reveal the changes of individual inter-molecular interacting pairs during the binding, including the native and non-native contact pairs. At the beginning of the binding process ($Q_{inter} < 0.1$), there are several non-native contacts between LF and PIP-box of DPO4 and PCNA2 monomer ([Figures S4A and S5A](#)). At this stage, these non-native contacts in the PCNA12–DPO4 complex are more and stronger than that in the PCNA123–DPO4 complex, which may be related to the flexibility of the PCNA12 dimer (see the next section). For DPO4 to PCNA123, the inter-molecular contacts with probability higher than 0.2 locate between residues 196, 302, and 304 of DPO4 (thumb and LF) and PCNA1. For DPO4 to PCNA12, contacts with similar strength change to locate between residues 301, 302, 304, 339, and 349 of DPO4 (LF and PIP-box) and PCNA1. It suggests that the initial complex formed at the beginning of DPO4 binding to PCNA123 is a bit different from that of DPO4 binding to PCNA12. The simulation results show that the mean binding time of DPO4 to PCNA123 (5.36τ) is a bit higher than that of DPO4 to PCNA12 (4.02τ). The interactions between PCNA12 and DPO4 at the beginning may favor the binding process. In addition, there are a few non-native contacts between LF of DPO4 and PCNA2 monomer at the I2 state of PCNA12–DPO4 binding, whereas these non-native contacts do not exist at the same stage of PCNA123–DPO4 binding (see [Figures S4D and S5D](#)). Besides, at the I2 state of both PCNA123–DPO4 and PCNA12–DPO4 binding processes, the palm domain of DPO4 has non-native contacts with the C terminus of PCNA1, which do not appear at the other stages of binding. At the B state of both PCNA123–DPO4 and PCNA12–DPO4 binding processes, DPO4 forms inter-molecular interactions with PCNA1 only, the same as that in PDB: 3FDS (see [Figure 1F](#)). At every stage of DPO4 binding to PCNA123 or PCNA12, contacts between DPO4 and PCNA mainly locate on the PCNA1 monomer. This is consistent with previous experimental results that PCNA1 is the minimum and sufficient DPO4-binding partner [Xing et al. \(2009\)](#).

PCNA12 Becomes Open and Twisted without PCNA3

The PCNA123 ring structure is closed and remains almost planar when it is isolated (see PDB: 2HII). In the previous experimental studies, it was found that the PCNA12 heterodimer becomes somewhat open and twisted when compared with PCNA123 ([Xing et al., 2009](#)). The DPO4 binding does not significantly affect the open conformation of the PCNA12 but marginally stabilizes the off-plane spiral conformation. Here we aim to quantify the different conformations of PCNA12 by calculating the angle and dihedral of the dimer. As illustrated in [Figure 6A](#), the interface between PCNA1 and PCNA2 (yellow cartoons) acts as the hinge of PCNA12 during this kind of conformational change. The angle of PCNA1(COM1)–hinge(COM2)–PCNA2(COM4) is defined as the opening angle of PCNA12 (θ_{12}); the dihedral of PCNA1(COM1)–hinge1(COM2)–hinge2(COM3)–PCNA2(COM4) is defined as the off-plane angle of PCNA12 (φ_{12}). For *apo* PCNA123 (PDB: 2HII), θ_{12} and φ_{12} are 102.678° and -0.592° . Without PCNA3, *apo* PCNA12 (PDB: 2IO4) has slightly higher θ_{12} (110.130°) and lower φ_{12} (-32.145°) than *apo* PCNA123. When PCNA12 is bound with DPO4 (PDB: 3FDS), θ_{12} changes slightly (109.888°), whereas φ_{12} becomes a little higher (-24.704°) compared with *apo* PCNA12.

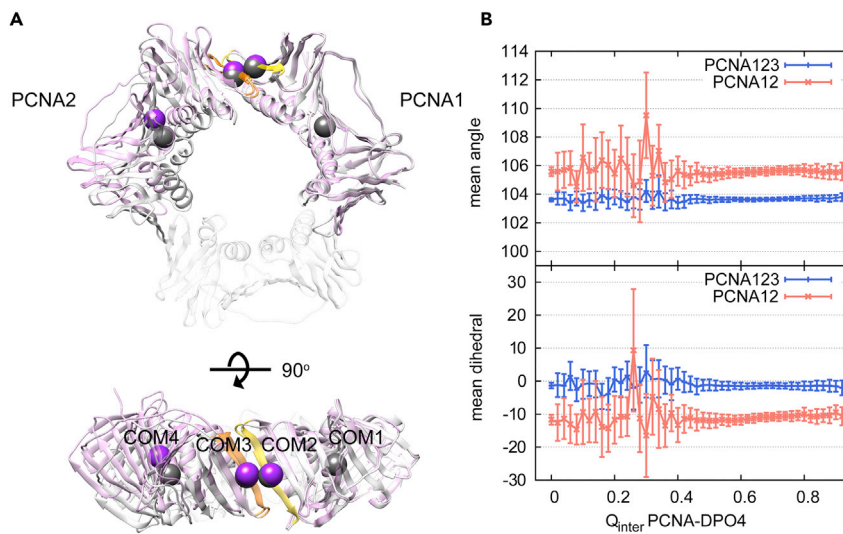


Figure 6. Changes of PCNA Planar

(A) Superimposed PCNA12 (DPO4-bound PCNA12 in 3FDS, colored pink) and PCNA123 (*apo* PCNA123 in PDB: 2H11, colored gray) with respect to PCNA1, as well as some beads indicating the center of mass (COM) of PCNA1 (COM1), hinge 1 (COM2, residues 175–183 of PCNA1), hinge 2 (COM3, residues 105–113 of PCNA2), and PCNA2 (COM4); (B) distribution of θ_{12} (angle COM1–COM2–COM4, top panel) and φ_{12} (dihedral COM1–COM2–COM3–COM4, bottom panel) on the binding paths of DPO4 to PCNA12 (pink) and PCNA123 (blue), with standard error value as error bar. Here mean angle/dihedral and its standard error have been calculated. The four beads (COM1, COM2, COM3, and COM4) of PCNA123 are colored gray and those of PCNA12 magenta. Since we aligned the two structures with respect to PCNA1, the two COM1 beads in these two structures are almost overlapped.

In our simulation, we collected all the θ_{12} and φ_{12} data during the binding process. As shown in Figure 6B, it is clear that the removal of PCNA3 will lead to an increase in the mean θ_{12} of about 2° and a decrease in the mean φ_{12} by about 10° . Whether DPO4 is bound or not, θ_{12} does not change significantly. Similar results can be obtained for PCNA123. However, the middle stage ($Q_{inter} \sim 0.1$ – 0.4) of DPO4 binding to PCNA12 exhibits much larger fluctuations in θ_{12} and φ_{12} than that of DPO4 binding to PCNA123. In addition, the θ_{12} of PCNA123 (with or without DPO4) is much more concentrated than that of PCNA12 (with or without DPO4, see Figure S6). These results suggest that PCNA3 may have a role in stabilizing the PCNA12 conformation. Moreover, φ_{12} of DPO4-bound PCNA123 is similar to that of unbound PCNA123. However, φ_{12} of DPO4-bound PCNA12 is slightly higher (by about 1°) than that of unbound PCNA12, which is consistent with the experimental structures. This also implies that PCNA3 may help maintain the PCNA planar conformation.

Limitations of the Study

Both the Y-family DNA polymerase IV (DPO4) and proliferating cell nuclear antigen (PCNA) are essential for DNA replication and translesion synthesis. However, the cooperation between DPO4 and PCNA and the movement of DPO4 on PCNA are still unclear. Here, based on a series structures of *apo* DPO4, *apo* PCNA, and the DPO4-PCNA complex, we have developed the structure-based coarse-grained model for both trimeric PCNA–DPO4 complex (PCNA123–DPO4) and dimeric PCNA–DPO4 complex (PCNA12–DPO4) and found three main states during DPO4 reaching PCNA ring. Here in this study, we did not incorporate the ligand DNA in our simulation model since there is no structure of DPO4-PCNA complexed with the ligand DNA, which is located in the center of the PCNA ring. Further molecular dynamics investigations based on the structure of DPO4-PCNA complexed with the ligand DNA will be in urgent need in the future.

Resource Availability

Lead Contact

Further information and requests for resources should be directed to and will be fulfilled by the Lead Contact, Jin Wang (jin.wang.1@stonybrook.edu).

Materials Availability

This study did not generate new unique reagents.

Data and Code Availability

All relevant data are available from the authors upon reasonable request.

METHODS

All methods can be found in the accompanying [Transparent Methods supplemental file](#).

SUPPLEMENTAL INFORMATION

Supplemental Information can be found online at <https://doi.org/10.1016/j.isci.2020.101117>.

ACKNOWLEDGMENTS

W.-T.C. thanks Network and Computing Center, Changchun Institute of Applied Chemistry, Chinese Academy of Science, and Computing Center of Jilin Province for computational support. W.-T.C. thanks the support from National Natural Science Foundation of China Grants 21603217 and 21721003, Youth Innovation Promotion Association CAS Grant 2020231, and Ministry of Science and Technology of the People's Republic of China Grant 2016YFA0203200. J.W. and Z.S. thank the support from National Institutes of Health Grant 1R01GM124177-01A1.

AUTHOR CONTRIBUTIONS

W.-T.C., Z.S., and J.W. designed research; W.-T.C. performed research; W.-T.C., Z.S., and J.W. analyzed data; and W.-T.C., Z.S., and J.W. wrote the paper.

DECLARATION OF INTERESTS

The authors declare no competing interests.

Received: December 26, 2019

Revised: March 22, 2020

Accepted: April 26, 2020

Published: May 22, 2020

REFERENCES

- Boudsocq, F., Kokoska, R.J., Plosky, B.S., Vaisman, A., Ling, H., Kunkel, T.A., Yang, W., and Woodgate, R. (2004). Investigating the role of the little finger domain of Y-family DNA polymerases in low fidelity synthesis and translesion replication. *J. Biol. Chem.* *279*, 32932–32940.
- Bryngelson, J.D., and Wolynes, P.G. (1987). Spin glasses and the statistical mechanics of protein folding. *Proc. Natl. Acad. Sci. U S A* *84*, 7524–7528.
- Chu, J.-W., and Voth, G.A. (2007). Coarse-grained free energy functions for studying protein conformational changes: a double-well network model. *Biophys. J.* *93*, 3860–3871.
- Chu, W.-T., Chu, X., and Wang, J. (2017). Binding mechanism and dynamic conformational change of C subunit of PKA with different pathways. *Proc. Natl. Acad. Sci. U S A* *114*, E7959–E7968.
- Chu, W.-T., and Wang, J. (2018). Quantifying the intrinsic conformation energy landscape topography of proteins with large-scale open-closed transition. *ACS Cent. Sci.* *4*, 1015–1022.
- Chu, X., Liu, F., Maxwell, B.A., Wang, Y., Suo, Z., Wang, H., Han, W., and Wang, J. (2014). Dynamic conformational change regulates the protein-DNA recognition: an investigation on binding of a Y-family polymerase to its target DNA. *PLoS Comput. Biol.* *10*, e1003804.
- Chu, X., and Wang, J. (2020). Theoretical investigations of a multi-domain protein folding under confinements and crowders. *Biophys. J.* *118*, 510a.
- Clementi, C., Nymeyer, H., and Onuchic, J.N. (2000). Topological and energetic factors: what determines the structural details of the transition state ensemble and “en-route” intermediates for protein folding? An investigation for small globular proteins. *J. Mol. Biol.* *298*, 937–953.
- Dalrymple, B.P., Kongsuwan, K., Wijffels, G., Dixon, N.E., and Jennings, P.A. (2001). A universal protein-protein interaction motif in the eubacterial DNA replication and repair systems. *Proc. Natl. Acad. Sci. U S A* *98*, 11627–11632.
- Demarest, S.J., Martinezyamout, M.A., Chung, J., Chen, H., Xu, W., Dyson, H.J., Evans, R.M., and Wright, P.E. (2002). Mutual synergistic folding in recruitment of CBP/p300 by p160 nuclear receptor coactivators. *Nature* *415*, 549–553.
- Dieckman, L.M., Freudenthal, B.D., and Washington, M.T. (2012). PCNA structure and function: insights from structures of PCNA complexes and post-translationally modified PCNA. *Subcell. Biochem.* *62*, 281–299.
- Dionne, I., Brown, N.J., Woodgate, R., and Bell, S.D. (2008). On the mechanism of loading the PCNA sliding clamp by RFC. *Mol. Microbiol.* *68*, 216–222.
- Dionne, I., Nookala, R.K., Jackson, S.P., Doherty, A.J., and Bell, S.D. (2003). A heterotrimeric PCNA in the hyperthermophilic archaeon *Sulfolobus solfataricus*. *Mol. Cell* *11*, 275–282.
- Dore, A.S., Kilkenny, M.L., Jones, S.A., Oliver, A.W., Roe, S.M., Bell, S.D., and Pearl, L.H. (2006). Structure of an archaeal PCNA1-PCNA2-FEN1 complex: elucidating PCNA subunit and client enzyme specificity. *Nucleic Acids Res.* *34*, 4515–4526.
- Friedberg, E.C., Wagner, R.P., and Radman, M. (2002). Specialized DNA polymerases, cellular survival, and the genesis of mutations. *Science* *296*, 1627–1630.

- Ganguly, D., Zhang, W., and Chen, J. (2013). Electrostatically accelerated encounter and folding for facile recognition of intrinsically disordered proteins. *PLoS Comput. Biol.* **9**, e1003363.
- Georgescu, R.E., Kim, S., Yurieva, O., Kuriyan, J., Kong, X., and Odonnell, M. (2008). Structure of a sliding clamp on DNA. *Cell* **132**, 43–54.
- Gulbis, J.M., Kelman, Z., Hurwitz, J., Odonnell, M., and Kuriyan, J. (1996). Structure of the C-terminal region of p21WAF1/CIP1 complexed with human PCNA. *Cell* **87**, 297–306.
- Kelman, Z. (1997). PCNA: structure, functions and interactions. *Oncogene* **14**, 629–640.
- Kumar, S., Bouzida, D., Swendsen, R.H., Kollman, P.A., and Rosenberg, J.M. (1992). The weighted histogram analysis method for free-energy calculations on biomolecules. I: the method. *J. Comput. Chem.* **13**, 1011–1021.
- Ling, H., Boudsocq, F., Woodgate, R., and Yang, W. (2001). Crystal structure of a Y-family DNA polymerase in action: a mechanism for error-prone and lesion-bypass replication. *Cell* **107**, 91–102.
- Ling, H., Boudsocq, F., Woodgate, R., and Yang, W. (2004). Snapshots of replication through an abasic lesion; structural basis for base substitutions and frameshifts. *Mol. Cell* **13**, 751–762.
- Liu, F., Chu, X., Lu, H.P., and Wang, J. (2017). Molecular mechanism of multispecific recognition of Calmodulin through conformational changes. *Proc. Natl. Acad. Sci. U S A* **114**, E3927–E3934.
- Lu, Q., and Wang, J. (2008). Single molecule conformational dynamics of adenylate kinase: energy landscape, structural correlations, and transition state ensembles. *J. Am. Chem. Soc.* **130**, 4772–4783.
- Matsumiya, S., Ishino, Y., and Morikawa, K. (2001). Crystal structure of an archaeal DNA sliding clamp: proliferating cell nuclear antigen from *Pyrococcus furiosus*. *Protein Sci.* **10**, 17–23.
- Noel, J.K., Whitford, P.C., and Onuchic, J.N. (2012). The shadow map: a general contact definition for capturing the dynamics of biomolecular folding and function. *J. Phys. Chem. B* **116**, 8692–8702.
- Noel, J.K., Whitford, P.C., Sanbonmatsu, K.Y., and Onuchic, J.N. (2010). SMOG@ ctbp: simplified deployment of structure-based models in GROMACS. *Nucleic Acids Res.* **38**, W657–W661.
- Ohmori, H., Friedberg, E.C., Fuchs, R.P.P., Goodman, M.F., Hanaoka, F., Hinkle, D.C., Kunkel, T.A., Lawrence, C.W., Livneh, Z., Nohmi, T., et al. (2001). The Y-family of DNA polymerases. *Mol. Cell* **8**, 7–8.
- Okazaki, K.-i., Koga, N., Takada, S., Onuchic, J.N., and Wolynes, P.G. (2006). Multiple-basin energy landscapes for large-amplitude conformational motions of proteins: structure-based molecular dynamics simulations. *Proc. Natl. Acad. Sci. U S A* **103**, 11844–11849.
- Pascal, J.M., Tsodikov, O.V., Hura, G.L., Song, W., Cotner, E.A., Classen, S., Tomkinson, A.E., Tainer, J.A., and Ellenberger, T. (2006). A flexible interface between DNA ligase and PCNA supports conformational switching and efficient ligation of DNA. *Mol. Cell* **24**, 279–291.
- Shoemaker, B.A., Portman, J.J., and Wolynes, P.G. (2000). Speeding molecular recognition by using the folding funnel: the fly-casting mechanism. *Proc. Natl. Acad. Sci. U S A* **97**, 8868–8873.
- Silvian, L.F., Toth, E.A., Pham, P., Goodman, M.F., and Ellenberger, T. (2001). Crystal structure of a DinB family error-prone DNA polymerase from *Sulfolobus solfataricus*. *Nat. Struct. Mol. Biol.* **8**, 984–989.
- Steitz, T.A. (1999). DNA polymerases: structural diversity and common mechanisms. *J. Biol. Chem.* **274**, 17395–17398.
- Trincao, J., Johnson, R.E., Escalante, C.R., Prakash, S., Prakash, L., and Aggarwal, A.K. (2001). Structure of the catalytic core of *S. cerevisiae* DNA polymerase η : implications for translesion DNA synthesis. *Mol. Cell* **8**, 417–426.
- Tsurimoto, T. (1999). PCNA binding proteins. *Front. Biosci.* **4**, 849–858.
- Turjanski, A.G., Gutkind, J.S., Best, R.B., and Hummer, G. (2008). Binding-induced folding of a natively unstructured transcription factor. *PLoS Comput. Biol.* **4**, e1000060.
- Uljon, S.N., Johnson, R.E., Edwards, T.A., Prakash, S., Prakash, L., and Aggarwal, A.K. (2004). Crystal structure of the catalytic core of human DNA polymerase kappa. *Structure* **12**, 1395–1404.
- Vladena, H., Guangxin, X., Jacob, B., Yoon, J.S., Isabelle, D., Kanagalaghatta, R.R., Stephen, D.B., and Hong, L. (2008). Structures of monomeric, dimeric and trimeric PCNA: PCNA-ring assembly and opening. *Acta Crystallogr. D Biol. Crystallogr.* **64**, 941–949.
- Waga, S., and Stillman, B. (1998). The DNA replication fork in eukaryotic cells. *Annu. Rev. Biochem.* **67**, 721–751.
- Wang, Y., Chu, X., Suo, Z., Wang, E., and Wang, J. (2012). Multidomain protein solves the folding problem by multifunnel combined landscape: theoretical investigation of a Y-family DNA polymerase. *J. Am. Chem. Soc.* **134**, 13755–13764.
- Warbrick, E. (2000). The puzzle of PCNA's many partners. *Bioessays* **22**, 997–1006.
- Whitford, P.C., Miyashita, O., Levy, Y., and Onuchic, J.N. (2007). Conformational transitions of adenylate kinase: switching by cracking. *J. Mol. Biol.* **366**, 1661–1671.
- Wong, J.H., Fiala, K.A., Suo, Z., and Ling, H. (2008). Snapshots of a Y-family DNA polymerase in replication: substrate-induced conformational transitions and implications for fidelity of Dpo4. *J. Mol. Biol.* **379**, 317–330.
- Xing, G., Kirouac, K., Shin, Y.J., Bell, S.D., and Ling, H. (2009). Structural insight into recruitment of translesion DNA polymerase Dpo4 to sliding clamp PCNA. *Mol. Microbiol.* **71**, 678–691.
- Yeh, I., Lee, M.S., and Olson, M.A. (2008). Calculation of protein heat capacity from replica-exchange molecular dynamics simulations with different implicit solvent models. *J. Phys. Chem. B* **112**, 15064–15073.
- Zhou, B.S., and Elledge, S.J. (2000). The DNA damage response: putting checkpoints in perspective. *Nature* **408**, 433–439.

iScience, Volume 23

Supplemental Information

Binding-Induced Conformational Changes Involved in Sliding Clamp PCNA and DNA Polymerase DPO4

Wen-Ting Chu, Zucui Suo, and Jin Wang

Supporting information

Binding-induced conformational changes involved in sliding clamp PCNA and DNA polymerase DPO4

Wen-Ting Chu¹, Zucui Suo², and Jin Wang^{3,*}

¹*State Key Laboratory of Electroanalytical Chemistry, Changchun Institute of Applied Chemistry, Chinese Academy of Sciences,
Changchun, Jilin, 130022, China*

²*Department of Biomedical Sciences, College of Medicine, Florida State University, Tallahassee, FL 32306-4300, USA*

³*Department of Chemistry & Physics, State University of New York at Stony Brook, Stony Brook, NY, 11794, USA*

**Corresponding Author: jin.wang.1@stonybrook.edu*

1 Transparent Methods

1.1 Initial model of simulation

The initial coarse-grained C_α structure-based models (SBM) were constructed for PCNA123–DPO4 and PCNA12–DPO4 complexes, by using SMOG on-line toolkit (Noel et al., 2010; Clementi et al., 2000; Noel et al., 2012; Lammert et al., 2009). This C_α model includes one bead on the C_α atom of each residue of the system. The model of heterotrimeric ring PCNA123 from *S. solfataricus* was generated from two PDB structures, 2HII (*apo S. sol* PCNA123) (Pascal et al., 2006) and 3FDS (*S. sol* PCNA12 with DPO4 bound) (Xing et al., 2009). Trimeric ring PCNA123 (2HII) contains PCNA1 (Met1-Leu249), PCNA2 (Met1-Ala245), and PCNA3 (Met1-Lys243). In addition, the model of the binding partner DPO4 was built from the 3FDS (PCNA-bound DPO4) and 2RDI (*apo* DPO4) (Wong et al., 2008). DPO4 is a 352 a.a. protein. Two-basin SBM was prepared for both PCNA123 trimer and DPO4, respectively, with the similar method used before (Chu and Voth, 2007; Chu et al., 2014; Wang et al., 2012b; Okazaki et al., 2006; Chu and Wang, 2018; Liu et al., 2017; Chu et al., 2017b). The key to construct a model with multiple basins is to build a mixed contact map which integrates multiple structural information together. In this work, all the intra-chain native contacts within PCNA (or within DPO4) can be collected into *core* (native contacts involved in both structures) and *specific* (native contacts involved in only one structure). All the inter-monomer native contacts within PCNA123 are obtained from 2HII. And the inter-chain native contacts between PCNA and DPO4 come from 3FDS.

The modeled two-basin Hamiltonian can be given as:

$$\begin{aligned} U &= U_{SBM}^{two-basin} + U_{charged} \\ &= U_{bonds} + U_{angles} + U_{dihedrals} + U_{LJ} + U_{charged} \end{aligned} \quad (S1)$$

For the local terms of the Hamiltonian, the bond term is expressed as $U_{bonds} = K_r(r - r_0)^2$. Here, K_r is the strength of the bond term, which is set to 100ε . For the large-scale conformational changes between native structures, the pseudo angle and dihedral terms are divided into non-hinge and hinge regions, by comparing the differences of angle and dihedral degrees in the native structures:

$$U_{angles} + U_{dihedrals} = U_{non-hinge} + K_{hinge}U_{hinge} \quad (S2)$$

, where $U_{non-hinge}$ and U_{hinge} have the same functional form (angles: $K_\theta(\theta - \theta_0)^2$; dihedrals: $K_\phi^{(1)}(1 - \cos(\phi - \phi_0)) + K_\phi^{(3)}(1 - \cos(3(\phi - \phi_0)))$). Here, θ_0 and ϕ_0 are the angle and dihedral values in the closed state. For non-hinge regions, $K_\theta = 20\varepsilon$, $K_\phi^{(1)} = \varepsilon$, $K_\phi^{(3)} = 0.5\varepsilon$. Hinge term, which is defined as before (Chu and Wang, 2018; Chu et al., 2017b, 2014), is set to control the flexibility of the model. In hinge regions, K_θ and K_ϕ are rescaled by 0.01, mimicking the flexibility.

The non-local term is in the form of Lennard-Jones (LJ) interactions, which can be divided into the term of native contacts (attractive, $U_{attractive}$) and the term of non-native contacts (repulsive, $U_{repulsive}$) within the protein ($U_{LJ} = U_{attractive} + U_{repulsive}$). All the native contacts were identified by the Shadow Algorithm (Noel et al., 2012). The expression of $U_{attractive}$ can be given as:

$$\begin{aligned} U_{attractive} &= K_{intra} * U_{LJ}(\gamma^{intra}) + K_{inter} * U_{LJ}(\gamma^{inter}) \\ &= K_{core} * U_{LJ}(\gamma^{core}) + K_{speci} * U_{LJ}(\gamma^{speci}) + K_{interP} * U_{LJ}(\gamma^{interP}) + K_{interD} * U_{LJ}(\gamma^{interD}) \end{aligned} \quad (S3)$$

, where the LJ attractive expression is $5 \left(\frac{\sigma_{ij}}{r_{ij}} \right)^{12} - 6 \left(\frac{\sigma_{ij}}{r_{ij}} \right)^{10}$. In this model, the $U_{attractive}$ term can be divided into intra-chain interaction terms and inter-chain interaction terms. The former includes the *core* part and the *specific* part. And the latter contains the potentials between PCNA monomers (*interP*) and between DPO4 and PCNA (*interD*). The parameter K_{core} values for PCNA123 and DPO4 are set to 2.0 and 3.0 (K_{speci} values for both PCNA123 and DPO4 are 1.5), respectively, in order to let PCNA123 and DPO4 have similar thermo-stability (see the next subsection). The repulsive interactions have the potential function as $K_{NC} \left(\frac{\sigma_{NC}}{r_{ij}} \right)^{12}$.

The electrostatic potential ($U_{charged}$) is computed by the *Debye – Hückel* model (Azia and Levy, 2009; Givaty and Levy, 2009; Chu et al., 2012; Wang et al., 2012a), which can be used to quantify the strength of the charge-charge attraction and repulsion in varying ion strengths:

$$U_{charged} = \Gamma_{DH} \times K_{coulomb} B(\kappa) \sum_{i,j} \frac{q_i q_j \exp(-\kappa r_{ij})}{\epsilon_r r_{ij}} \quad (S4)$$

In Eq. S4, $K_{coulomb} = 4\pi\epsilon_0 = 138.94 \text{kJ} \cdot \text{mol}^{-1} \cdot \text{nm} \cdot \text{e}^{-2}$ is the electric conversion factor; $B(\kappa)$ is the salt-dependent coefficient; κ^{-1} is the Debye screening length, which is directly influenced by the solvent ion strength (IS)/salt concentration C_{salt} ($\kappa \approx 3.2\sqrt{C_{salt}}$); ϵ_r is the dielectric constant, which was set to 80 during the simulations. Γ_{DH} is the energy scaled coefficient for balancing the total energy. In our model, Lys and Arg have a positive point charge (+e), Asp and Glu have a negative point charge (-e). All the charges are placed on the C_α atoms. In the physiological salt concentration ($C_{salt} = 0.15M$), κ is 1.24nm^{-1} . As a result, we set $\Gamma_{DH} = 0.535$ in our simulations, in order to have V_{DH} for two opposite charged atoms located at a distance of 0.5 nm equal to the native contact energy. Here in our simulations, physiological salt concentration ($C_{salt} = 0.15M$) was set as the simulated ionic strength. When a native contact is an ionic pair (salt bridge), we rescaled its interaction strength by 0.1 so that its energetic contribution will be comparable to other native contacts (Levy et al., 2007).

1.2 Parameter calibration

In this study, we use coarse-grained structure-based model to investigate the conformational changes during the binding process of DPO4 to PCNA123/PCNA12. As a result, the simulation temperature is not the same as the real temperature (Clementi et al., 2000; Lammert et al., 2009). In our previous studies, we compared the simulated folding temperature and the experimental melting temperature of a protein. And then the simulated room temperature was determined according to the ratio of melting temperature and room temperature (Chu et al., 2017b,a). However, there are no experimental results about the melting temperature of PCNA (PCNA123 or PCNA12) or DPO4 available. Therefore, we calculated the folding temperature values of PCNA1, PCNA2, PCNA3, and DPO4, as well as the binding temperature between PCNA1 and PCNA2, between PCNA2 and PCNA3, between PCNA1 and PCNA3. First of all, the K_{core} of PCNA123 was set to 2.0 and the K_{core} of DPO4 was tuned to make sure that both PCNA123 and DPO4 are stable at room temperature. After a series of REMD simulations, we found that when K_{core} of DPO4 is 3.0, DPO4 has similar thermo-stability as PCNA123 (see Fig. S1). The folding temperature (T_f) of PCNA123 is about 2.29 (in reduced unit), and the T_f of DPO4 is about 2.19. While within PCNA123, the T_f of PCNA1 (2.28) is similar as that of PCNA2 (2.27), but higher than that of PCNA3 (2.14).

Then we set K_{interP} to 1.0 (the parameters between PCNA1 and PCNA2, PCNA1 and PCNA3, PCNA2 and PCNA3 are the same). We can also recognize the binding temperature T_b between the two monomers of PCNA123 (as shown in Fig. S1B). The T_b values between PCNA1 and PCNA2, between PCNA1 and PCNA3, between PCNA2 and PCNA3 are 1.73, 1.69 and 1.70, respectively. Therefore, the interactions between PCNA1 and PCNA2 are slightly stronger than that between PCNA1 and PCNA3, between PCNA2 and PCNA3. According to the heat capacity curves of PCNA123 and DPO4, we set the simulation temperature 1.24 (about 149 K in Gromacs) corresponds to the room temperature (about $0.7 T_b$), in order to ensure the stability of PCNA ring at room temperature. In our model, the binding energy between PCNA1 and PCNA2 is higher than that between PCNA3 and PCNA1 or between PCNA3 and PCNA2, which is consistent with the experimental findings that the interactions between PCNA1 and PCNA2 is stronger than others (Dionne et al., 2003).

We next tuned the parameter K_{interD} between PCNA and DPO4 to 2.0, after building the PCNA–DPO4 complex system. With this setting, the system is occupied with DPO4 bound state at room temperature (Fig. S1).

1.3 MD simulation

All simulations were performed with Gromacs 4.5.5 (Hess et al., 2008). The coarse grained molecular dynamics simulations (CGMD) used Langevin equation with constant friction coefficient $\gamma = 1.0$. The cutoff for non-bonded interactions was set to 3.0 nm. The MD time step was set to 0.5 fs and the trajectories were saved every 10 ps. To enhance the sampling of binding events, a strong harmonic potential was added if the distance between the center of mass of PCNA

and DPO4 is greater than 8.0 nm (Tribello et al., 2014).

For thermodynamic simulations, REMD simulations with 28 replicas were performed on both PCNA123–DPO4 and PCNA12–DPO4 systems to overcome the energy barriers between unbound and bound states. The initial conformations of the two systems are at unbound state. That is, we put DPO4 (from 3FDS) and PCNA123/PCNA12 (from 2HII) at distance of about 6.0 nm to ensure that they do not have interactions at the beginning of REMD simulations. Then the profiles of free energy curve or surface can be obtained by using WHAM algorithm (Kumar et al., 1992, 1995).

For kinetic simulations, 200 individual MD runs started with varying unbound configurations and velocities were performed on PCNA123–DPO4 and PCNA12–DPO4 systems, respectively. Each kinetic run starts from the unbound state ends to the bound state. Likewise, at the beginning, DPO4 was put far away from PCNA123/PCNA12 at distance of about 6.0 nm to 8 nm. These procedures make sure that DPO4 binds to PCNA123/PCNA12 in different directions.

We define that a native contact is formed if the $C\alpha$ - $C\alpha$ distance between any given native atom pair is within 1.2 times of its native distance. And a non-native contact is considered to be formed if the distance between the two beads of a contact pair is within 10 Å. For each kinetic run, the binding time (the first passage time of binding, FPT_{on}) equals to the simulation time of reaching the bound state firstly. Since the simulated binding time is different from the experimental binding time, we collected the FPT_{on} values in the unit of τ ($\tau = 1$ ns).

2 Supplemental Figures

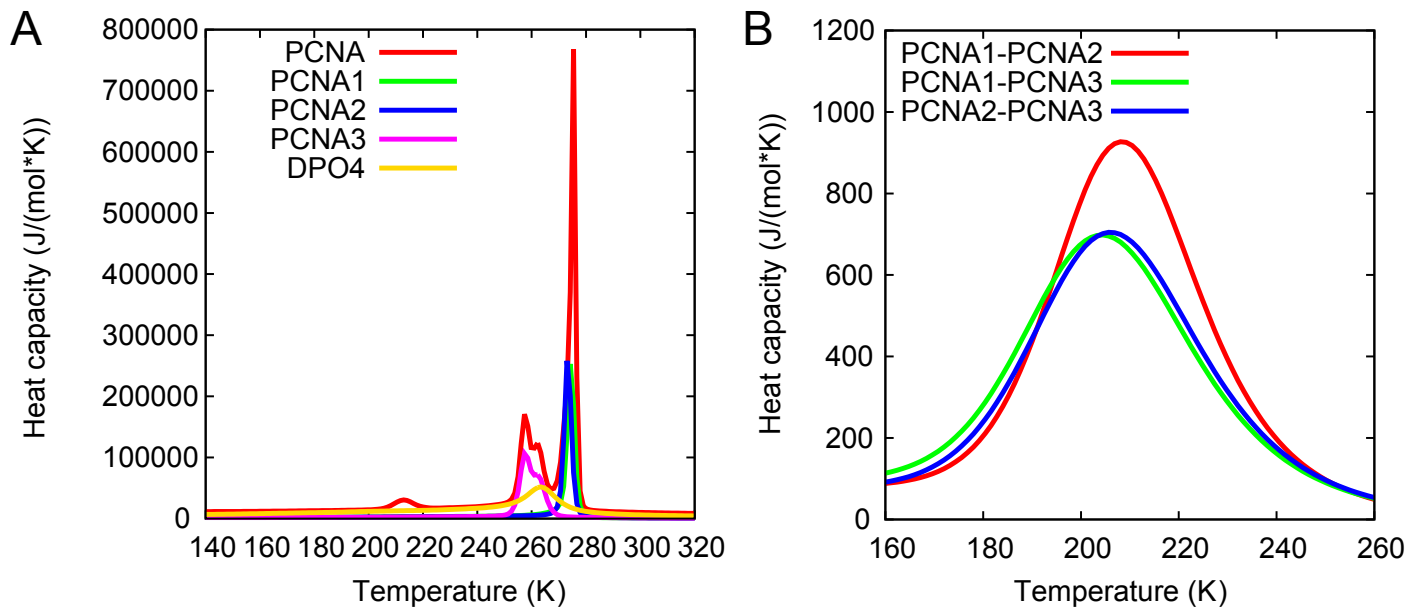


Fig. S1 Related to Figure 2. (A) The heat capacity curves of *apo* PCNA123 (red) and *apo* DPO4 (gold) as a function of temperature, as well as the heat capacity curves of PCNA1 (green), PCNA2 (blue), and PCNA3 (magenta) in *apo* PCNA123. (B) The heat capacity curves of the interactions between PCNA1 and PCNA2 (red), PCNA1 and PCNA3 (green), PCNA2 and PCNA3 (blue) as a function of temperature. Here the temperature in these coarse-grained SBM simulations is different from the real temperature.

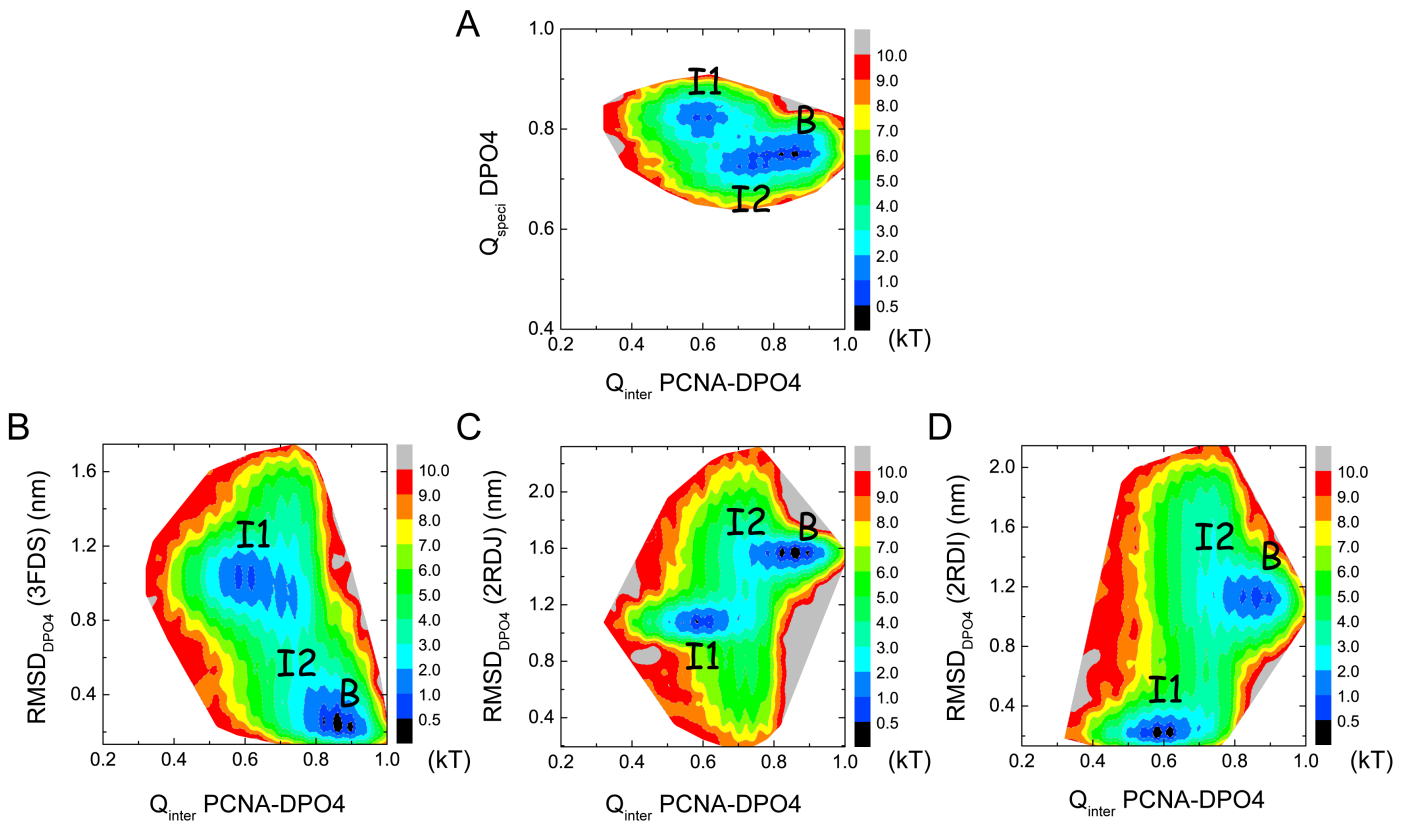


Fig. S2 Related to Figure 2. The free energy profile as a function of (A) the fraction of native contacts between PCNA and DPO4 ($Q_{\text{inter PCNA-DPO4}}$) and the fraction of specific native contacts of DPO4 ($Q_{\text{speci DPO4}}$), (B) $Q_{\text{inter PCNA-DPO4}}$ and RMSD of DPO4 with respect to the DPO4 in 3FDS ($RMSD_{\text{DPO4}}$ (3FDS)), (C) $Q_{\text{inter PCNA-DPO4}}$ and RMSD of DPO4 with respect to the DPO4 in 2RDJ ($RMSD_{\text{DPO4}}$ (2RDJ)), (D) $Q_{\text{inter PCNA-DPO4}}$ and RMSD of DPO4 with respect to the DPO4 in 2RDI ($RMSD_{\text{DPO4}}$ (2RDI)). These free energy data were extracted at $T = 1.24$ (in reduced unit, mimicking the room temperature).

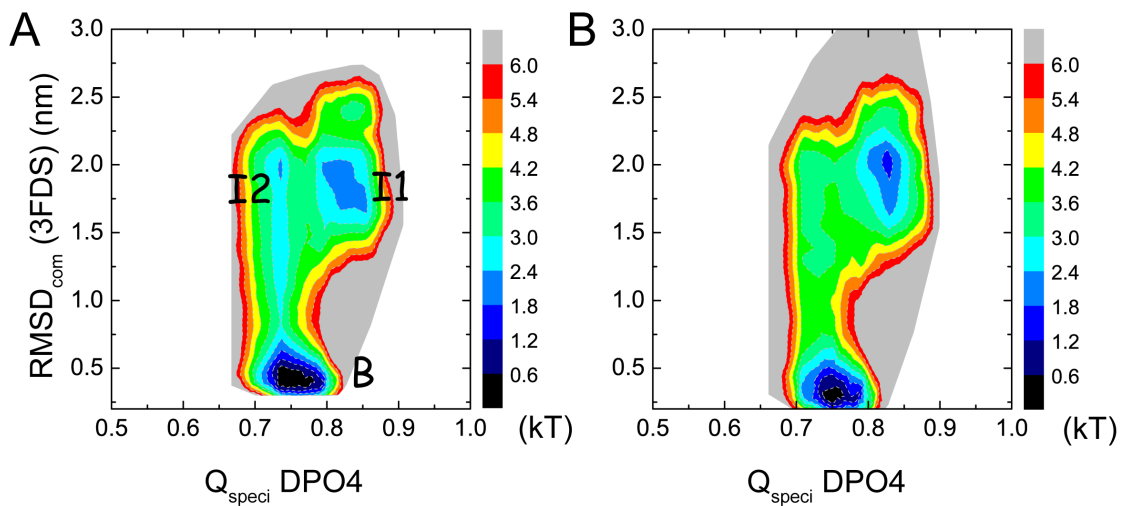


Fig. S3 Related to Figure 2. The free energy profile as a function of specific native contacts of DPO4 ($Q_{\text{speci DPO4}}$) and RMSD of PCNA12-DPO4 with respect to 3FDS ($RMSD_{\text{com}} (3FDS)$) in the system PCNA123-DPO4 (A) and PCNA12-DPO4 (B). These free energy data were extracted at $T = 1.24$ (in reduced unit, mimicking the room temperature).

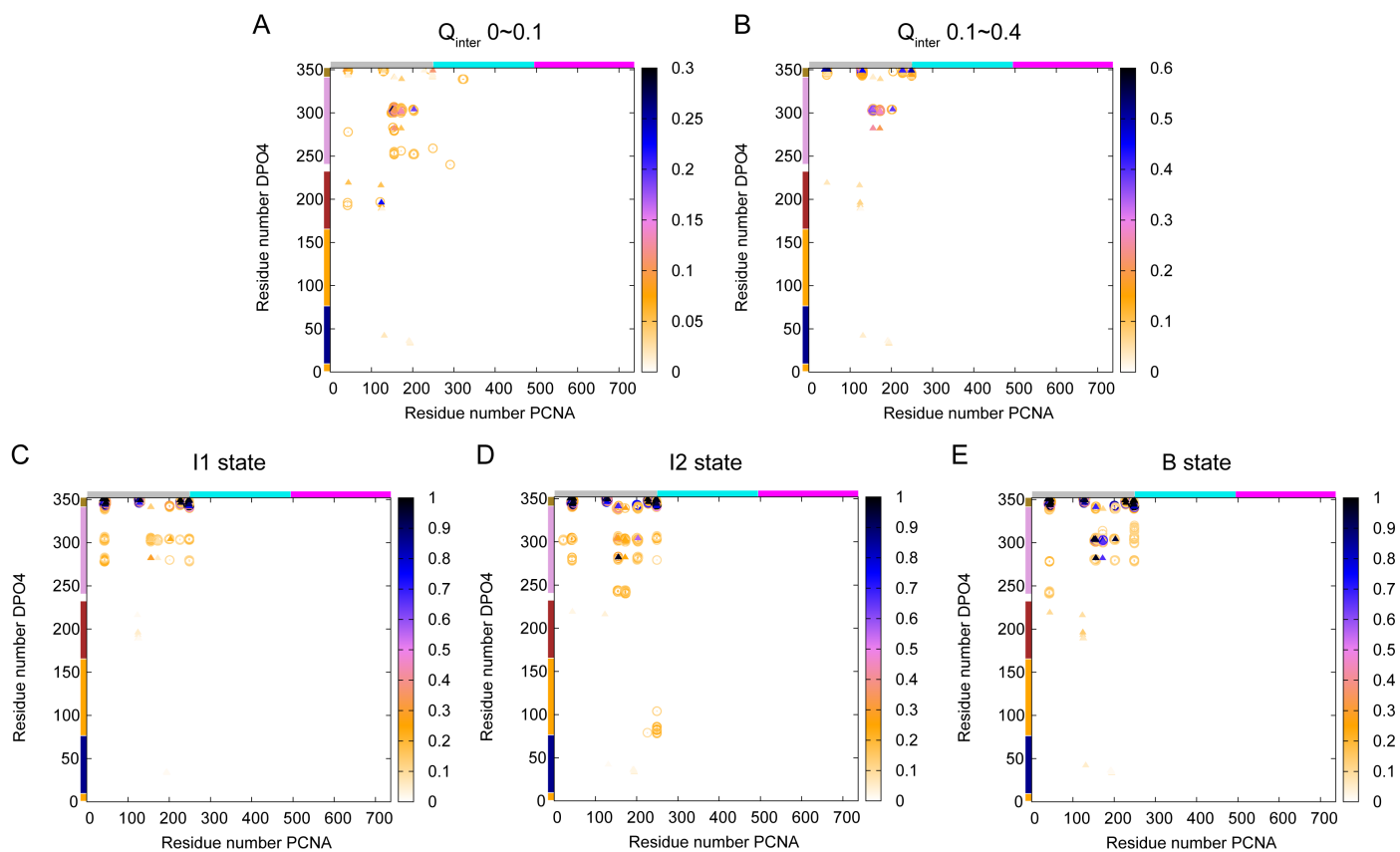


Fig. S4 Related to Figure 5. The evolution of the contact map between PCNA123 and DPO4 during the binding path. Each native and non-native contacts are illustrated with a triangle and a circle. The probability of each contact is shown with gradient color. The PCNA1 (1–249, gray), PCNA2 (250–494, cyan), and PCNA3 (495–737, magenta) are labeled along the x axis. The domains of DPO4 are labeled along the y axis with the same color as in Fig. 1. Here a non-native contact is considered to be formed if the distance between the two beads of a contact pair is within 10 Å.

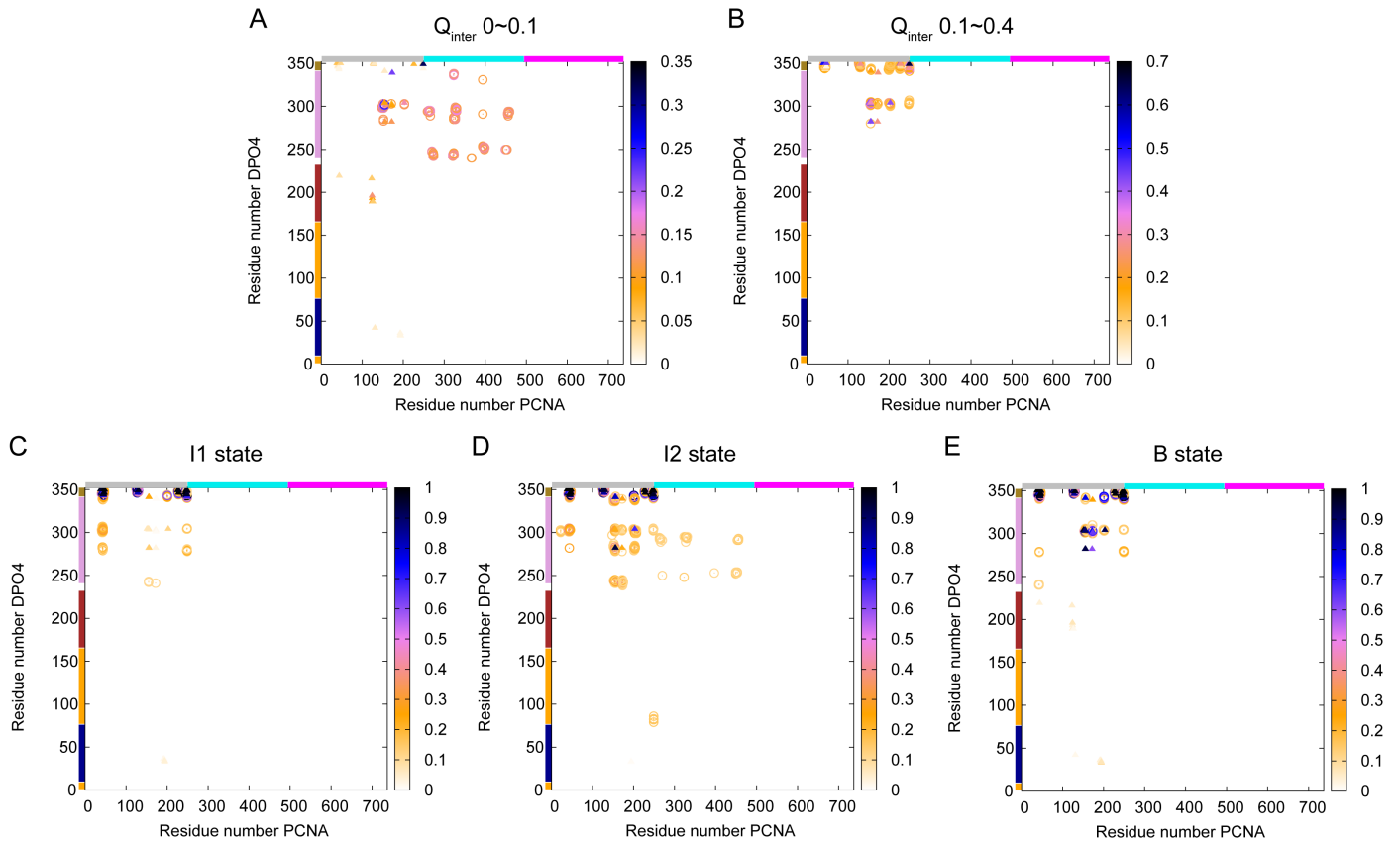


Fig. S5 Related to Figure 5. The evolution of the contact map between PCNA12 and DPO4 during the binding path. Each native and non-native contacts are illustrated with a triangle and a circle. The probability of each contact is shown with gradient color. The PCNA1 (1–249, gray), PCNA2 (250–494, cyan), and PCNA3 (495–737, magenta) are labeled along the x axis. The domains of DPO4 are labeled along the y axis with the same color as in Fig. 1. Here a non-native contact is considered to be formed if the distance between the two beads of a contact pair is within 10 Å.

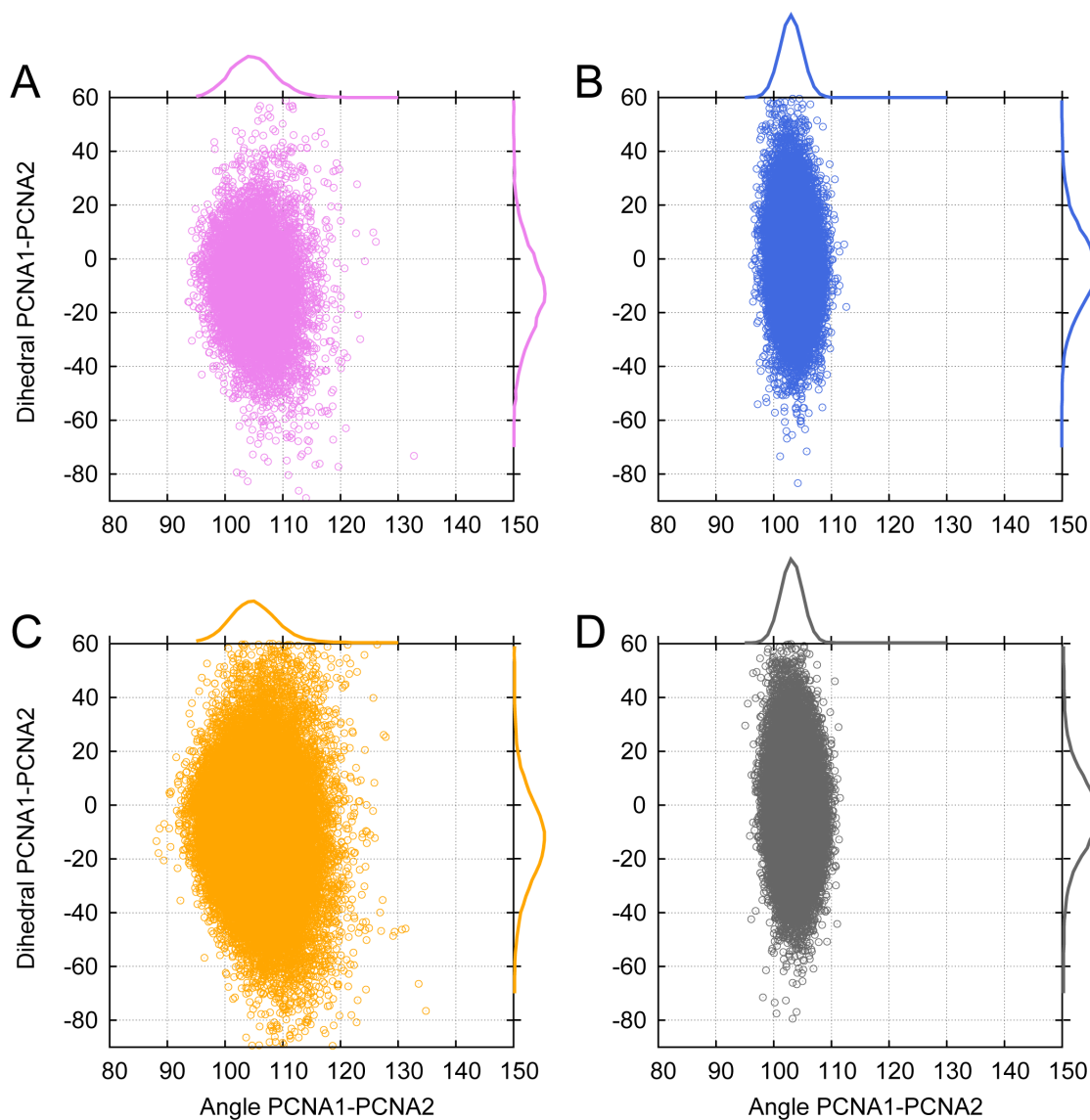


Fig. S6 Related to Figure 6. Distribution of both θ_{12} (horizontal axis) and φ_{12} (vertical axis) at unbound state of PCNA12 (A) and PCNA123 (B), and at bound state of PCNA12 (C) and PCNA123 (D). Note that the numbers of data points in the four panels are not the same.

References

- Azia, A. and Levy, Y. (2009). Nonnative electrostatic interactions can modulate protein folding: molecular dynamics with a grain of salt. *J. Mol. Biol.* *393*, 527–542.
- Chu, J.-W. and Voth, G. A. (2007). Coarse-grained free energy functions for studying protein conformational changes: a double-well network model. *Biophys. J.* *93*, 3860–3871.
- Chu, W., Clarke, J., Shammass, S. L. and Wang, J. (2017a). Role of non-native electrostatic interactions in the coupled folding and binding of PUMA with Mcl-1. *PLoS Comput. Biol.* *13*, e1005468.
- Chu, W.-T., Chu, X. and Wang, J. (2017b). Binding mechanism and dynamic conformational change of C subunit of PKA with different pathways. *Proc. Natl. Acad. Sci. U. S. A.* *114*, E7959–E7968.
- Chu, W.-T. and Wang, J. (2018). Quantifying the Intrinsic Conformation Energy Landscape Topography of Proteins with Large-Scale Open–Closed Transition. *ACS Cent. Sci.* *4*, 1015–1022.
- Chu, X., Liu, F., Maxwell, B. A., Wang, Y., Suo, Z., Wang, H., Han, W. and Wang, J. (2014). Dynamic Conformational Change Regulates the Protein-DNA Recognition: An Investigation on Binding of a Y-Family Polymerase to Its Target DNA. *PLoS Comput. Biol.* *10*, e1003804.
- Chu, X., Wang, Y., Gan, L., Bai, Y., Han, W., Wang, E., Wang, J. et al. (2012). Importance of electrostatic interactions in the association of intrinsically disordered histone chaperone Chz1 and histone H2A. Z-H2B. *PLoS Comput. Biol.* *8*, e1002608.
- Clementi, C., Nymeyer, H. and Onuchic, J. N. (2000). Topological and energetic factors: what determines the structural details of the transition state ensemble and "en-route" intermediates for protein folding? An investigation for small globular proteins. *J. Mol. Biol.* *298*, 937–953.
- Dionne, I., Nookala, R. K., Jackson, S. P., Doherty, A. J. and Bell, S. D. (2003). A heterotrimeric PCNA in the hyperthermophilic archaeon *Sulfolobus solfataricus*. *Mol. Cell* *11*, 275–282.
- Givaty, O. and Levy, Y. (2009). Protein sliding along DNA: dynamics and structural characterization. *J. Mol. Biol.* *385*, 1087–1097.
- Hess, B., Kutzner, C., Van Der Spoel, D. and Lindahl, E. (2008). GROMACS 4: algorithms for highly efficient, load-balanced, and scalable molecular simulation. *J. Chem. Theory Comput.* *4*, 435–447.

- Kumar, S., Rosenberg, J. M., Bouzida, D., Swendsen, R. H. and Kollman, P. A. (1992). The weighted histogram analysis method for free-energy calculations on biomolecules. I. The method. *J. Comput. Chem.* *13*, 1011–1021.
- Kumar, S., Rosenberg, J. M., Bouzida, D., Swendsen, R. H. and Kollman, P. A. (1995). Multidimensional free-energy calculations using the weighted histogram analysis method. *J. Comput. Chem.* *16*, 1339–1350.
- Lammert, H., Schug, A. and Onuchic, J. N. (2009). Robustness and generalization of structure-based models for protein folding and function. *Proteins: Struct., Funct., Bioinf.* *77*, 881–891.
- Levy, Y., Onuchic, J. N. and Wolynes, P. G. (2007). Fly-casting in protein-DNA binding: frustration between protein folding and electrostatics facilitates target recognition. *J. Am. Chem. Soc.* *129*, 738–739.
- Liu, F., Chu, X., Lu, H. P. and Wang, J. (2017). Molecular mechanism of multispecific recognition of Calmodulin through conformational changes. *Proc. Natl. Acad. Sci. U. S. A.* *114*, E3927–E3934.
- Noel, J. K., Whitford, P. C. and Onuchic, J. N. (2012). The shadow map: a general contact definition for capturing the dynamics of biomolecular folding and function. *J. Phys. Chem. B* *116*, 8692–8702.
- Noel, J. K., Whitford, P. C., Sanbonmatsu, K. Y. and Onuchic, J. N. (2010). SMOG@ ctbp: simplified deployment of structure-based models in GROMACS. *Nucleic Acids Res.* *38*, W657–W661.
- Okazaki, K.-i., Koga, N., Takada, S., Onuchic, J. N. and Wolynes, P. G. (2006). Multiple-basin energy landscapes for large-amplitude conformational motions of proteins: Structure-based molecular dynamics simulations. *Proc. Natl. Acad. Sci. U. S. A.* *103*, 11844–11849.
- Pascal, J. M., Tsodikov, O. V., Hura, G. L., Song, W., Cotner, E. A., Classen, S., Tomkinson, A. E., Tainer, J. A. and Ellenberger, T. (2006). A flexible interface between DNA ligase and PCNA supports conformational switching and efficient ligation of DNA. *Mol. Cell* *24*, 279–291.
- Tribello, G. A., Bonomi, M., Branduardi, D., Camilloni, C. and Bussi, G. (2014). PLUMED 2: New feathers for an old bird. *Comput. Phys. Commun.* *185*, 604–613.
- Wang, Y., Gan, L., Wang, E. and Wang, J. (2012a). Exploring the dynamic functional landscape of adenylate kinase modulated by substrates. *J. Chem. Theory Comput.* *9*, 84–95.
- Wang, Y., Tang, C., Wang, E. and Wang, J. (2012b). Exploration of multi-state conformational dynamics and underlying global functional landscape of maltose binding protein. *PLoS Comput. Biol.* *8*, e1002471.

- Wong, J. H., Fiala, K. A., Suo, Z. and Ling, H. (2008). Snapshots of a Y-family DNA polymerase in replication: substrate-induced conformational transitions and implications for fidelity of Dpo4. *J. Mol. Biol.* *379*, 317–330.
- Xing, G., Kirouac, K., Shin, Y. J., Bell, S. D. and Ling, H. (2009). Structural insight into recruitment of translesion DNA polymerase Dpo4 to sliding clamp PCNA. *Mol. Microbiol.* *71*, 678–691.